Dynamics of two mutually coupled semiconductor lasers: Instantaneous coupling limit

Serhiy Yanchuk*
Weierstrass Institute for Applied Analysis and Stochastics, Mohrenstrasse 39, D-10117 Berlin, Germany and Institute of Mathematics, Humboldt-University of Berlin, Unter den Linden 6, D-10099 Berlin, Germany

Klaus R. Schneider†
Weierstrass Institute for Applied Analysis and Stochastics, Mohrenstrasse 39, D-10117 Berlin, Germany

Lutz Recke‡
Humboldt-University of Berlin, Institute of Mathematics, Unter den Linden 6, D-10099 Berlin, Germany
(Received 12 November 2003; revised manuscript received 5 February 2004; published 25 May 2004)

We consider two semiconductor lasers coupled face to face under the assumption that the delay time of the injection is small. The model under consideration consists of two coupled rate equations, which approximate the coupled Lang-Kobayashi system as the delay becomes small. We perform a detailed study of the synchronized and antisynchronized solutions for the case of identical systems and compare results from two models: with the delay and with instantaneous coupling. The bifurcation analysis of systems with detuning reveals that self-pulsations appear via bifurcations of stationary (i.e., continuous wave) solutions. We discover the connection between stationary solutions in systems with detuning and synchronous (also antisynchronous) solutions of coupled identical systems. We also identify a codimension 2 bifurcation point as an organizing center for the emergence of chaotic behavior.

DOI: 10.1103/PhysRevE.69.056221 PACS number(s): 05.45.Xt, 42.55.Px

I. INTRODUCTION

The goal of the present paper is to study nonlinear dynamics of two mutually coupled semiconductor lasers. We consider the face to face configuration, i.e., the output of each laser is injected into the other laser. The study of such coupling setup is motivated among other facts by the perspective of using masked signal transmission [1,2] as well as investigation of the dynamics of two-section laser devices [3]. In addition to the application perspectives for the specific devices, models for coupled lasers turn out to be sources for new physical phenomena such as anticipated or lag synchronization, and chaos appearance for already weak coupling since the isolated lasers operate in a stable stationary regime. From the general perspective of coupled nonlinear oscillators [4], coupled semiconductor lasers usually are modeled by coupled systems with additional symmetry properties which have to be taken into account. Moreover, the significant difference between carrier and photon lifetimes brings multiscale properties into the models.

The dynamics of mutually coupled lasers with large injection feedback time (corresponding to distances from about 10 cm between the lasers) was studied recently in Ref. [5–7]. The case of unidirectional coupling was investigated in Ref. [8,9]. Various new phenomena were reported such as retarded or anticipated synchronization [10–13], inverse synchronization [14], localized synchronization [6], and antisynchronization of power drop outs [15].

Recently, there has been new interest in lasers with a short cavity [16], which is motivated by several arguments: First, the study of the dynamics in this regime has become experimentally accessible. Also, such a regime is very interesting from the dynamical point of view, since it has an intermediate complexity, allowing to analyze directly the mechanisms of either synchronization or the appearance of pulsations and chaotic dynamics. The same arguments seem to be applicable when the delay in the coupling is small, i.e., there is a *short external cavity*. For instance, this is the case in a two-section integrated device [3], where both lasers are parts of the same device and are close to each other *a priori*. The instantaneous coupling limit may serve as an appropriate starting point for the study of such systems. Of course, the smallness of the delay, which allows one to neglect it, is a separate question. When neglecting the delay in the amplitude terms, it turns out to be important to take into account the propagation phase φ caused by the delay. In order to see this, we take the optical frequency $\nu_{op} \sim 10^{14}$Hz and the relaxation frequency $\nu_r \sim 10^9$ Hz. If, for example, the length of the external cavity is 1 mm, then the propagation phase can be estimated as $\varphi \sim 10^{-3} \times 2\pi\nu_{op}/3 \times 10^8 \sim 10^3$ while the phase change of the slow amplitude will be $\varphi_A \sim 10^{-3} \times 2\pi\nu_r/3 \times 10^8 \sim 10^{-2}$ and can be neglected. From the more general perspective it is still an open problem of modeling: what kind of phenomena in the coupled face to face lasers can be described at least qualitatively by instantaneously coupled rate equations?

It is the main purpose of the present paper to give a comprehensive description of the dynamical regimes arising in a model of instantaneously coupled rate equations. For the case of identical lasers, we provide analytical conditions for the stability of synchronized and antisynchronized regimes, where the injection phase shift is the key parameter to determine the dynamics. Similar calculations are compared for

*Email address: yanchuk@wias-berlin.de
†Email address: schneider@wias-berlin.de
‡Email address: recke@mathematik.hu-berlin.de

two models: the model with small delay and that with instantaneous coupling. Further, we consider the case when there is a detuning between two lasers. It is shown how the injection phase affects the existence and stability of continuous wave solutions and of self-pulsations. It follows that one of the organizing centers for chaotic dynamics is a codimension -2 zero-Hopf bifurcation point.

II. THE MODEL

The model, which is extensively used to describe the dynamics of mutually coupled single-mode lasers (cf. Refs. [5,9,8,17]), is the system of coupled rate equations:

$$\begin{aligned}
\frac{dE_1}{dt} &= i\bar{\delta}E_1 + \frac{1}{2}\left(\mathcal{G}_1(N_1,|E_1|^2) - \frac{1}{\tau_{p_1}}\right)E_1 + \kappa e^{-i\varphi}E_2(t-\bar{\tau}),\\
\frac{dN_1}{dt} &= I_1 - \frac{N_1}{\tau_{c_1}} - \mathrm{Re}[\mathcal{G}_1(N_1,|E_1|^2)]|E_1|^2,\\
\frac{dE_2}{dt} &= \frac{1}{2}\left(\mathcal{G}_2(N_2,|E_2|^2) - \frac{1}{\tau_{p_2}}\right)E_2 + \kappa e^{-i\varphi}E_1(t-\bar{\tau}),\\
\frac{dN_2}{dt} &= I_2 - \frac{N_2}{\tau_{c_2}} - \mathrm{Re}[\mathcal{G}_2(N_2,|E_2|^2)]|E_2|^2,
\end{aligned} \tag{1}$$

where $E_{1,2}$ and $N_{1,2}$ denote the complex optical fields and the carrier densities of the lasers, respectively. The term $i\bar{\delta}E_1$ accounts for the frequency detuning. By $I_{1,2}$ we denote the pumping current, and $\mathcal{G}_{1,2}(N_{1,2},|E_{1,2}|^2)$ is the complex gain function. $\tau_{p_{1,2}}$, and $\tau_{c_{1,2}}$ are photon and carrier lifetimes; κ and τ characterize the injection rate and the injection delay time, respectively. The coupling strength κ should be small enough in order to perturb weakly the longitudinal resonances of the system. We do not address this question quantitatively, since it can be resolved only using multi-mode models as, for example, in Ref. [18], and may be device specific.

In system (1), we introduce the following simplifications and rescalings. First of all, we assume that all parameters for both lasers are the same except the detuning parameter $\bar{\delta}$. Neglecting nonlinear gain saturation we linearize the complex gain function as follows:

$$\mathcal{G}(N,|E|^2) - \frac{1}{\tau_p} := G_N(1+i\alpha)(N-N_0).$$

With the rescaling $E_{\mathrm{new}} = \sqrt{G_N\tau_c}E$, $N_{\mathrm{new}} = \frac{1}{2}\tau_p G_N(N-N_0)$, $t_{\mathrm{new}} = t/\tau_p$ we obtain from Eq. (1),

$$\begin{aligned}
E_1' &= i\delta E_1 + (1+i\alpha)N_1E_1 + \eta e^{-i\varphi}E_2(t-\tau),\\
N_1' &= \varepsilon[J - N_1 - (N_1+\nu)|E_1|^2],\\
E_2' &= (1+i\alpha)N_2E_2 + \eta e^{-i\varphi}E_1(t-\tau),\\
N_2' &= \varepsilon[J - N_2 - (N_2+\nu)|E_2|^2],
\end{aligned} \tag{2}$$

where we use the same notations for the new variables. The differentiation is assumed to be made with respect to the new time, and the parameters are

$$\eta = \tau_p\kappa, \quad \varepsilon = \tau_p/\tau_c, \quad J = \tau_p G_N(I\tau_c - N_0)/2,$$

$$\tau = \bar{\tau}/\tau_p, \quad \nu = 0.5, \quad \delta = \bar{\delta}\tau_p.$$

Note that $\kappa = r/\tau_{in}$, where r^2 is the fraction of the power injected from one laser to another and τ_{in} is the diode cavity round-trip time (cf. Refs. [19,20]). Therefore $\eta = r\tau_p/\tau_{in}$. Taking values $\tau_{in} = 8$ ps and $\tau_p = 2$ ps as for InGaAsP long wavelength laser diode (cf. Ref. [19]) we obtain that $\eta \approx r/4$. This relation is useful to have in mind for physical interpretation of the bifurcation diagrams and dynamical regimes described in the paper.

In the case $\tau = 0$, we obtain the coupled rate equations with instantaneous coupling:

$$\begin{aligned}
E_1' &= i\delta E_1 + (1+i\alpha)N_1E_1 + \eta e^{-i\varphi}E_2,\\
N_1' &= \varepsilon[J - N_1 - (N_1+\nu)|E_1|^2],\\
E_2' &= (1+i\alpha)N_2E_2 + \eta e^{-i\varphi}E_1,\\
N_2' &= \varepsilon[J - N_2 - (N_2+\nu)|E_2|^2].
\end{aligned} \tag{3}$$

System (3) is the main object of this study. In Sec. VII we compare some of the obtained results with the model (2) which includes small delay.

III. SYMMETRIES: SYNCHRONOUS AND ANTISYNCHRONOUS SOLUTIONS

Let us first examine the model (3) without detuning, i.e., $\delta = 0$, and note some properties due to inherent symmetries:

$$\begin{aligned}
E_j' &= (1+i\alpha)N_jE_j + \eta e^{-i\varphi}E_{3-j},\\
N_j' &= \varepsilon[J - N_j - (N_j+\nu)|E_j|^2], \quad j = 1,2.
\end{aligned} \tag{4}$$

(1) Since the subsystems are identical, there is a symmetry with respect to indices interchange $(E_1,N_1,E_2,N_2) \to (E_2,N_2,E_1,N_1)$. This implies that the invariant subspace of synchronous states $E_1 = E_2$ and $N_1 = N_2$ is invariant with respect to the flow corresponding to Eq. (4).

(2) The symmetry $(E_1,N_1,E_2,N_2) \to (-E_2,N_2,-E_1,N_1)$ implies the existence of the invariant subspace of antisynchronous states $E_1 = -E_2$ and $N_1 = N_2$.

(3) The following symmetry allows us to establish a one-to-one correspondence between synchronous and antisynchronous solutions. If $(E_1(t),N_1(t),E_2(t),N_2(t))$ is a solution to (4) then $(E_1(t),N_1(t),-E_2(t),N_2(t))$ is also a solution provided φ is replaced by $\varphi+\pi$. In other words, the symmetry transformation is of the form $(E_1(t),N_1(t),E_2(t),N_2(t),\varphi) \to (E_1(t),N_1(t),-E_2(t),N_2(t),\varphi+\pi)$. This implies that all antisynchronous solutions and their properties can be obtained from the corresponding synchronous solutions and their

properties, which have to be considered for the same parameter values except that φ is shifted by π.

Let us remark that the coupling, which is present in Eq. (4), influences the dynamics in the synchronization and antisynchronization subspaces. This, in particular, makes our situation different from the setup in Refs. [4,21].

The phase-shift invariance $(E_1,N_1,E_2,N_2) \rightarrow (E_1e^{i\psi},N_1,E_2e^{i\psi},N_2)$ is common to optical devices without phase conjugation, and, in particular, to the system (2) for any parameter δ and η. This symmetry implies that for suitable laser parameters there exist continuous wave (cw) solutions, i.e., solutions of the type $E_j(t)=E_{0_j}e^{i\omega t}, N_j=N_{0_j}$ $(j=1,2;\omega\in\mathbb{R})$. These solutions are also called "stationary," because they correspond to stationary intensity regimes. Moreover, this symmetry implies that for suitable laser parameters there exist modulated wave (MW) solutions, i.e., solutions of the type $E_j(t)=E_{0_j}(t)e^{i\omega t}, N_j=N_{0_j}(t)$ with $E_{0_j}(t+T)=E_{0_j}(t)$ and $N_{0_j}(t+T)=N_{0_j}(t)$ for all $t\in\mathbb{R}$ $(j=1,2;\omega,T\in\mathbb{R})$. These solutions are also called "periodic" or "self-pulsations", because they correspond to time-periodic intensity regimes.

IV. SYNCHRONOUS cw SOLUTIONS AND THEIR STABILITY

A. Dynamics in the synchronization subspace

After substituting $N_1=N_2=:N$ and $E_1=E_2=:E$ into Eq. (4), we obtain the following equations for the dynamics in the synchronization subspace:

$$E' = (1+i\alpha)NE + \eta e^{-i\varphi}E,$$
$$N' = \varepsilon[J-N-(N+\nu)|E|^2]. \tag{5}$$

A qualitative analysis of Eq. (5) with $\varepsilon>0$ and $\nu>0$ yields the following:

(a) For $\eta\cos\varphi<-J$ the "off state" $E=0$, $N=J$ is asymptotically stable.

(b) For $-J<\eta\cos\varphi<\nu$, there exists a globally stable cw solution $E(t)=E_0e^{i\omega_0 t}$, $N(t)=N_0$ with

$$\omega_0 = -\eta(\alpha\cos\varphi+\sin\varphi), \quad N_0 = -\eta\cos\varphi,$$
$$E_0 = (J+\eta\cos\varphi)/(\nu-\eta\cos\varphi).$$

Summarizing, let us note that for all physically relevant parameter values, i.e., $J>0$, $\varepsilon>0$, $0<\eta<\nu=0.5$, there exists a unique stable cw solution inside the subspace of synchronous solutions. The same is true for the subspace of antisynchronous solutions.

B. Transverse stability of the synchronous cw solutions

Since the synchronous cw solution is stable within the synchronization subspace, its stability in the whole phase space is determined by its *transverse* stability, i.e., the stability with respect to perturbations transverse to the synchronization subspace. The analysis of the transverse stability of synchronous cw solutions can be carried out by inspecting the characteristic equation

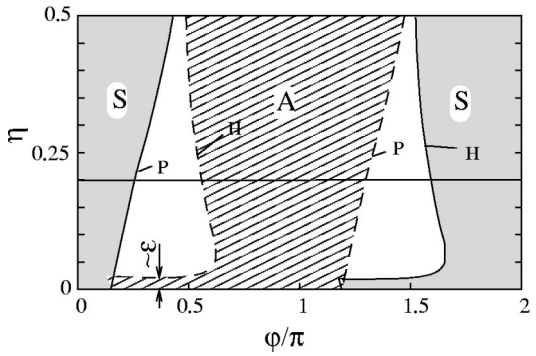

FIG. 1. Region of transverse stability for synchronous S and antisynchronous A cw solutions, respectively. P denotes the curves of transverse pitchfork bifurcations and H Hopf bifurcations for the parameters $\alpha=2$, $J=1$, $\varepsilon=0.03$.

$$\chi_T^0(\Lambda) = [\Lambda^2+4\Lambda\eta\cos\varphi+4\eta^2][\Lambda+\varepsilon(1+S_0)] + 2\varepsilon S_0(\nu-\eta\cos\varphi)[\Lambda+2\eta(\cos\varphi-\alpha\sin\varphi)] = 0, \tag{6}$$

where

$$S_0 := \frac{J+\eta\cos\varphi}{\nu-\eta\cos\varphi}.$$

This equation is derived in Appendix A. We shall note that the roots of $\chi_T^0(\Lambda)=0$ determine only transverse stability of the synchronous cw solutions, since the general characteristic equation can be factorized into two equations one of which corresponding to transverse directions and another to the directions within the synchronization subspace, cf. Appendix A. Transverse pitchfork bifurcation takes place if there is a zero eigenvalue, i.e., $\chi_T^0(0)=0$, and transverse Hopf bifurcation corresponds to the existence of pure imaginary eigenvalues, i.e., $\chi_T^0(i\Omega)=0$, where $\Omega\neq 0$ is some real parameter. These bifurcations can be identified and path followed with respect to the system parameters. Here we choose the coupling strength η and injection phase φ to be the key parameters with respect to which we want to study the dynamics. Typical bifurcation diagram is shown in Fig. 1. The figure shows regions for transverse stability of the synchronous cw solution (marked by S) and antisynchronous cw solution (marked by A), respectively. Note that in order to obtain the result for antisynchronous solutions, we used the symmetry arguments of Sec. III, i.e., the region A is an image of the region S, which is shifted by π along the parameter axis φ. The transverse bifurcations that mediate the loss of synchronization are marked as P for pitchfork and H for Hopf, respectively. Note that we do not show in Fig. 1 all the bifurcation lines, but only those which mediate the stability loss of cw solutions.

There are also small regions where stable synchronous and stable antisynchronous cw solutions coexist. They are located at $\varphi=\arctan(1/\alpha)$ and $\varphi=\arctan(1/\alpha)+\pi$ and their size is of order ε, cf. Fig. 2.

The bifurcation diagrams, cf. Figs. 1 and 2, also reveal that the first destabilization threshold, i.e., destabilization of

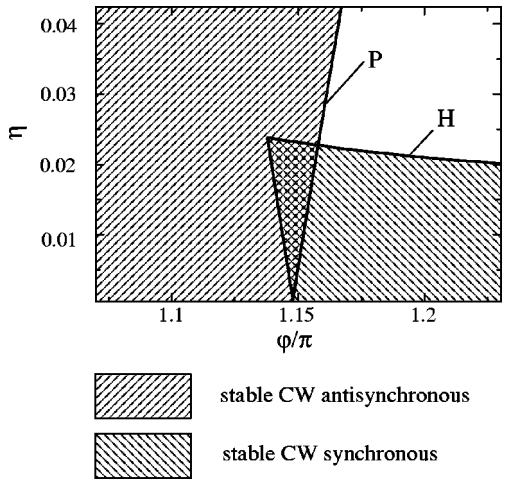

FIG. 2. Zoom of the small part of Fig. 1. The regions of stability of synchronous and antisynchronous cw solutions are overlapped, creating multistability. Here the bifurcation curves are shown completely, i.e., not only those parts that bounds the stability regions of the corresponding cw solutions.

the cw solutions with increasing of the coupling η for fixed φ, may occur already for coupling strength of order ε via Hopf bifurcation.

V. ASYNCHRONOUS cw SOLUTIONS

Synchronous and antisynchronous cw solutions are not the only possible stationary solutions in the system (4). Another set of cw solutions, which we call *asynchronous*, can be obtained from the following ansatz:

$$E_1(t) = a_1 e^{i(\omega t+\psi)}, \quad N_1(t) = N_1 = \text{const},$$
$$E_2(t) = a_2 e^{i\omega t}, \quad N_2(t) = N_2 = \text{const}, \tag{7}$$

where $a_1, a_2, N_1, N_2, \omega, \psi$ are real constants to be determined. After substituting it into Eq. (4), we obtain a set of nonlinear equations, which afterward can be effectively studied numerically. We refer the reader to Appendix B for details. As a result we present the one-dimensional bifurcation diagram in Fig. 3, which corresponds to the parameters as in Fig. 1 but with fixed $\eta=0.2$ (cf. horizontal line in the figure). In addition to the synchronous and antisynchronous solutions, we observe branches of unstable asynchronous orbits connecting synchronous and antisynchronous cw solutions. These branches emerge from the subcritical pitchfork bifurcations P_s and P_a, respectively. Although these solutions are unstable their role may be important in forming the boundary of the attracting region of stable synchronous cw solutions.

In the following section, we study system (3) for $\delta \neq 0$, i.e., we investigate the influence of the detuning.

VI. INFLUENCE OF THE DETUNING

A. Preliminary study

Since system (3) has the phase-shift invariance property, we can reduce it to a five-dimensional system. One way of

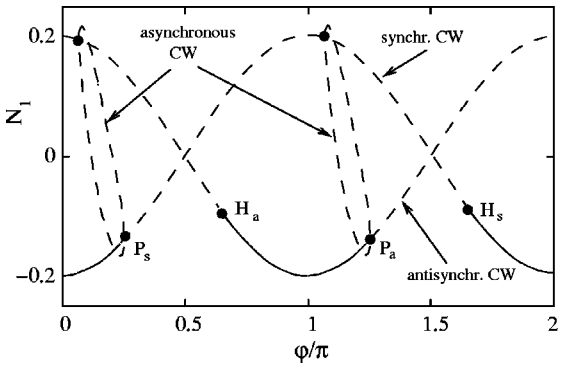

FIG. 3. For fixed $\eta=0.2$, there are two branches corresponding to the synchronous and antisynchronous solutions and the connecting branches of unstable asynchronous unstable periodic solutions. P_a and P_s are pitchfork and H_a, H_s are Hopf bifurcations. Index s stands for the synchronous and a for antisynchronous solutions, respectively.

reducing is to use the following transformation: $E_1(t) = a_1(t)e^{i\psi_1(t)}$, $E_2(t) = a_2(t)e^{i\psi_2(t)}$. Here a_1^2 and a_2^2 are intensities of the first and the second laser, respectively. We assume $a_1 \neq 0$ and $a_2 \neq 0$. $\Delta\psi = \psi_1 - \psi_2$ is their phase difference. Then with respect to the new real variables a_1, a_2, N_1, N_2, and $\Delta\psi$ we obtain the system of equations

$$\begin{aligned} a_1' &= N_1 a_1 + \eta a_2 \cos(\Delta\psi + \varphi), \\ N_1' &= \varepsilon[J - N_1 - (N_1 + \nu)a_1^2], \\ a_2' &= N_2 a_2 + \eta a_1 \cos(\varphi - \Delta\psi), \\ N_2' &= \varepsilon[J - N_2 - (N_2 + \nu)a_2^2], \\ \Delta\psi' &= \delta + (N_1 - N_2)\alpha - \eta\frac{a_2}{a_1}\sin(\Delta\psi + \varphi) + \eta\frac{a_1}{a_2}\sin(\varphi - \Delta\psi). \end{aligned} \tag{8}$$

System (8) no longer possess the phase-shift symmetry, and, therefore, all cw solutions become stationary states and all MW solutions become periodic (if $\Delta\psi$ is considered modulo 2π) in terms of new variables.

Let us introduce the frequencies Ω_1 and Ω_2 by

$$\Omega_1(t) = \psi_1'(t), \quad \Omega_2(t) = \psi_2'(t).$$

The following quantity is often used to determine the locking between two weakly coupled oscillators:

$$\Delta\overline{\Omega} = \langle \Delta\psi'(t) \rangle = \lim_{T\to\infty} \frac{1}{T}\int_0^T \Delta\psi'(t)dt = \lim_{T\to\infty} \frac{\Delta\psi(T)}{T}.$$

$\Delta\overline{\Omega}$ can be treated as averaged frequency difference between two weakly coupled lasers.

Figure 4 shows results of computation of $\Delta\overline{\Omega}$ depending on the detuning δ. Three different curves were obtained for different values of φ with fixed $\eta=0.3$. At each point, we integrated over the transient interval $T_{\text{tr}}=1000$ and averaged over $T_{\text{av}}=1000$. Initial conditions were chosen at random.

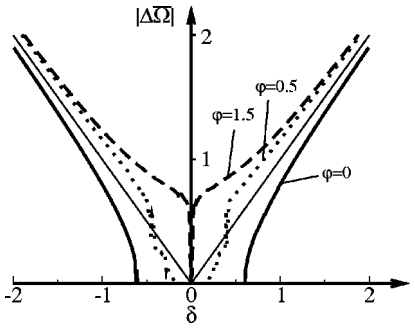

FIG. 4. Averaged frequency difference vs detuning parameter for different values of φ (η=0.3).

One clearly observes the locking intervals $\Delta\overline{\Omega}=0$ as plateaus near $\delta=0$. Moreover, the width of these intervals strongly depend on the phase parameter φ. We will inspect the dependence of the locking on φ in more details in the following sections by studying bifurcations that are involved in the loss of locking and appearance of pulsations. Additionally, we have to note that the use of frequency difference $\Delta\overline{\Omega}$ for investigating of the locking between two coupled oscillators can be justified in the case of weak coupling, i.e., small enough η. Therefore, we have to consider Fig. 4 as a preliminary result, which has to be accompanied by an additional bifurcation analysis in the following sections.

B. Stationary states for the case with detuning

The cw solutions of system (3) are equilibria of system (8). Hence, one can use the standard path-following technique to follow their dependence on the parameters. As starting data, we use the known stationary states for the symmetric system (see Fig. 3). The resulting bifurcation diagram is shown in Fig. 5, which is computed for the detuning $\delta=0.1$. Before analyzing the obtained bifurcation diagrams, it is important to realize that detuning breaks two symmetries in our system (cf. Sec. III): $\mathbb{Z}_2$ symmetry $(E_1,N_1,E_2,N_2)\rightarrow(E_2,N_2,E_1,N_1)$ and the symmetry $(E_1,N_1,E_2,N_2)\rightarrow(-E_2,N_2,-E_1,N_1)$. Therefore, exactly synchronous and exactly antisynchronous solutions do not exist anymore. Moreover, the pitchfork bifurcations that partially determine the synchronization region of the system without detuning is no longer admissible for $\delta\neq 0$. Two questions arise naturally: What happens with the synchronous and antisynchronous solutions after the symmetry breaking by detuning? How is the pitchfork bifurcation perturbed in this case? The observed scenario, cf. Fig. 5, clarifies the situation. In particular, as can be seen from Fig. 5(b), instead of the pitchfork bifurcation we have a saddle-node bifurcation (denoted as "LP"). In the nonsymmetric case this saddle-node bifurcation connects the previously synchronous solutions via the unstable branch of asynchronous solutions to the antisynchronous, cf. Fig. 5(a). Note that such a perturbation of the pitchfork bifurcation is common for symmetrically coupled systems with a parameter mismatch [22]. As a result, instead of the separate branches of synchronous and antisynchronous solutions, for $\delta\neq 0$ there are closed branches of solutions, which do not

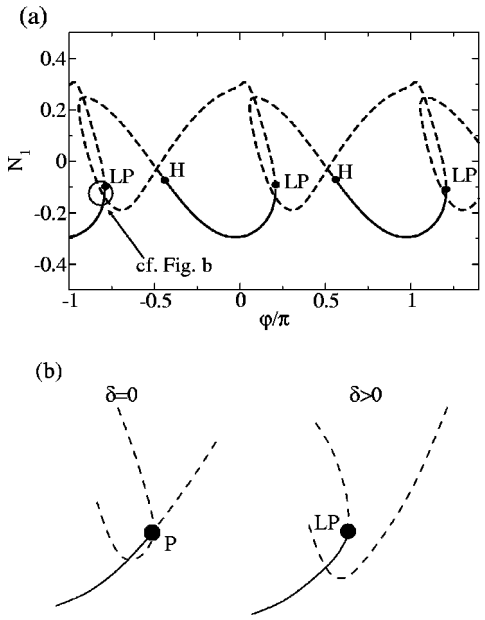

FIG. 5. (a) Stationary states for system (3) with detuning. $\delta=0.01$, $\eta=0.2$. Stable branches are depicted by solid lines, unstable by dashed. (b) Perturbation of the pitchfork bifurcation by the detuning, zooming of some part of (a).

possess these symmetry properties. Nevertheless, as we shall see in Sec. VI D, some parts of these branches still keep being close to the synchronous state and some to the antisynchronous.

Comparing the bifurcation diagram in Fig. 5 and its symmetric counterpart in Fig. 3 we note that similar stability regions for stationary states, which are limited by the Hopf (H) and saddle-node (LP) bifurcations, exist in both cases. In fact, they can be obtained from each other by continuation along the parameter δ. Moreover, as we will see in Sec. VI D, the corresponding branches are close to the synchronous (those that contain $\varphi=0$) and to the antisynchronous one (containing $\varphi=\pm 1$). It is evident that for these stationary states correspond to $\Delta\psi(t)=$const. In the following, by the locking between coupled systems with detuning (3) we understand the existence of the stable stationary states, i.e., CW solutions (for them we have $\Delta\psi=$const).

C. Regions of locking

The only parameter in our model, which induces mismatch between the lasers is the detuning δ. In order to study the influence of δ on stable frequency-locked states, we investigate the boundaries of the stability region, i.e., the bifurcation points LP and H in Fig. 5(a), depending on δ. The resulting bifurcation diagram is shown in Fig. 6. There we denote by D_s and D_a two regions, corresponding to the existence of stable stationary states. We distinguish between these two regions because the first one is connected to the synchronous stationary states and the second one to the antisynchronous at $\delta=0$. For more details about these states we refer to the following section. The Hopf bifurcation line is marked by black color and the saddle-node bifurcation by gray.

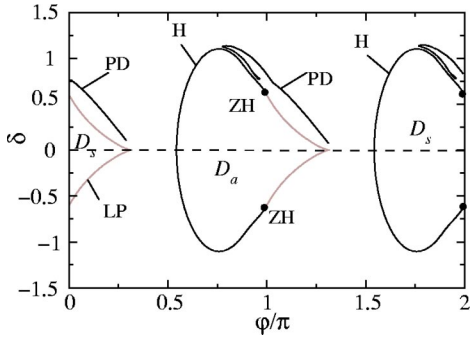

FIG. 6. Stability regions for the stationary states of coupled systems with detuning. LP and H denotes saddle-node and Hopf bifurcations, respectively. ZH is a codimension-2 zero-Hopf (or Guckenheimer-Gavrilov) bifurcation point. PD—period-doubling bifurcation curve for rotations of Eq. (8).

Note that the diagram in Fig. 6 is obtained for fixed coupling strength η. Another way of representation is to consider detuning δ and coupling strength η as the active parameters. Figure 7 shows such bifurcation diagrams for fixed values of φ. The different values of φ correspond to qualitatively different bifurcation diagrams. The regions of stability of cw solutions are marked by gray color. As it is expected, for sufficiently small coupling η in Figs. 7(a)–7(c), the stability region is bounded by saddle-node bifurcation lines. For $\varphi=-0.84$ and $\varphi=1.41$, in addition to saddle-node bifurcation mechanism, Hopf bifurcation lines appear to confine partially the locking regions. The codimension-2 bifurcation points (ZH) appear where Hopf and saddle-node bifurcation lines meet.

The symmetry of the bifurcation diagrams in Figs. 6 and 7 with respect to interchange $\delta\rightarrow-\delta$ can be explained by the fact that system (3) is invariant under the following transformation $(E_1,E_2,N_1,N_2,\delta)\rightarrow(E_2e^{i\delta t},E_1e^{i\delta t},N_2,N_1,-\delta)$.

D. Properties of the stationary states after the symmetry breaking

By definition, cw solutions have the form

$$E_1(t)=a_1e^{i(\omega t+\Delta\psi)},\quad E_2(t)=a_2e^{i\omega t},$$

$$N_1(t)=N_1=\text{const},\quad N_2(t)=N_2=\text{const}.$$

Now we show that their particular shape, i.e., the values of $a_1,a_2,\Delta\psi$, is influenced by the symmetry that is broken by the detuning δ. Particularly, in the region D_s (see Fig. 6) we have stationary solutions that are close in some sense to synchronous and in the region D_a close to antisynchronous states. This becomes clear when one notes that the region D_s contains the set of synchronous states when $\delta=0$ and D_a contains antisynchronous states. In other words, as $\delta\rightarrow0$ the stable locked solutions from the region D_s continuously approach the synchronous cw states and from D_a the antisynchronous, respectively. For the synchronous solutions one has $a_1/a_2=1$ and $\Delta\psi=0$ and antisynchronous $a_1/a_2=1$ and $\Delta\psi=\pm\pi$. As an example, we plot in Fig. 8 the ratio of amplitudes a_1/a_2 and a phase shift $\Delta\psi$ as a function of φ for $\delta=0.2$, i.e., parameters belong to D_s.

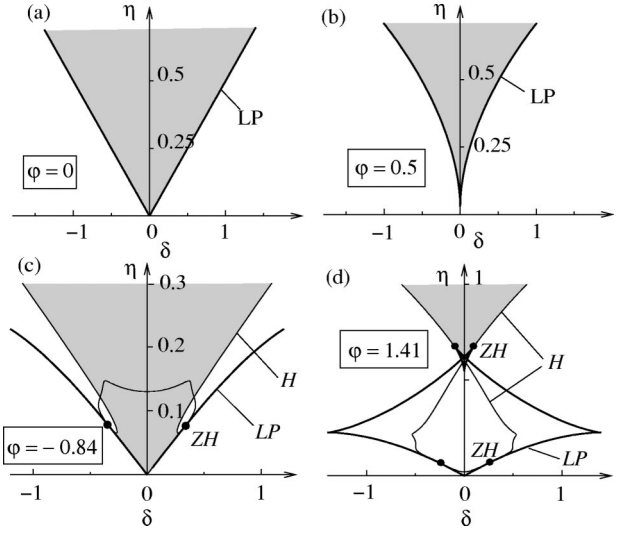

FIG. 7. Bifurcation diagrams with respect to coupling strength η and detuning δ for fixed $\varphi=0$ (a), $\varphi=0.5$ (b), $\varphi=-0.84$, $\varphi=1.41$. Hopf bifurcations H are denoted by thin lines and saddle-nodes LP by more heavy lines. Stability regions for stationary states are marked in gray. ZH are zero-Hopf (or Guckenheimer-Gavrilov) bifurcation points of codimension 2.

E. Self-pulsations

Self-pulsations, i.e., periodic oscillations of the field intensity, appear as a result of the Hopf bifurcation of the stationary locked states. In terms of the original system (3) they are invariant tori, while for system (9) these solutions become either a periodic solutions, or rotations, which are periodic with respect to the variables a_1,a_2,N_1,N_2 but with unbounded variable $\Delta\psi$ such that $\Delta\psi(t+T)=\Delta\psi(t)+2k\pi$ with some integer k. Such solutions can be studied either

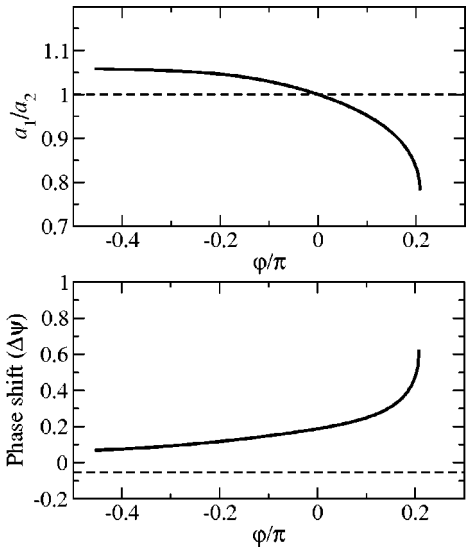

FIG. 8. Characteristics of some locked solutions from the region D_s of Fig. 6.

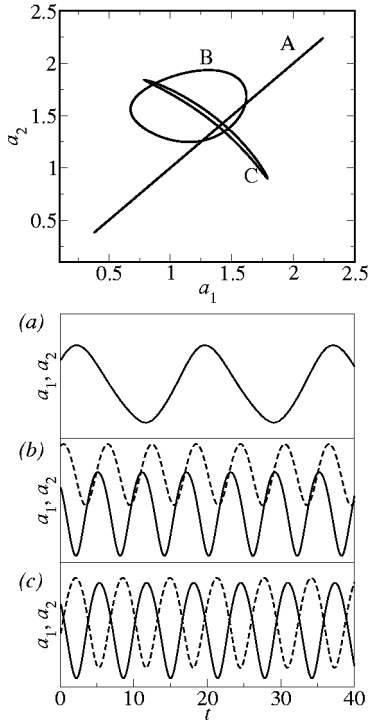

FIG. 9. Different types of self-pulsations. (a), (b), and (c) show time dependence of the amplitudes a_1 and a_2 of both lasers. The corresponding parameter values: $\delta=0.7$, $\varphi=0$ (a), $\varphi=\pi/4$ (b), and $\varphi=\pi/2$ (c).

directly by AUTO continuation software [23] or can be treated as bounded limit cycles after appropriate coordinate transformation, which allows us to consider $\Delta\psi$ modulo 2π. Both approaches allow one to make bifurcation analysis of such solutions. In this way we detected a period-doubling bifurcation, which, together with a Hopf bifurcation of the stationary solutions, restrict the region where stable self-pulsations occur, cf. Fig. 6.

We have noticed that near the period-doubling bifurcation self-pulsations appear, which are close to the diagonal in the space (a_1,a_2), cf. Fig. 9, orbit *A*. Such pulsations appear when there is no phase shift between the amplitudes a_1 and a_2 of the lasers, cf. Fig. 9(a). On the contrary, near the Hopf bifurcation, we observe that self-pulsations are close to the "antidiagonal." Such a phenomenon was reported in Ref. [14] and called "inverse synchronization." In this case, a_1 is shifted with respect to a_2 by a half of the period, cf. Fig. 9(c). The orbit *B* in Fig. 9 corresponds to the intermediate regime. In the following two sections we consider these phenomena in more detail and show that the phase propagation parameter φ determines the possibility to observe identical or inverse amplitude synchronization.

F. Identical amplitude synchronization

It is a remarkable fact that coupled systems with detuning (8) still admit solutions for which the amplitudes behave identically, i.e., $a_1=a_2$. An example of such a solution is shown in Fig. 9(a). The necessary condition for the existence

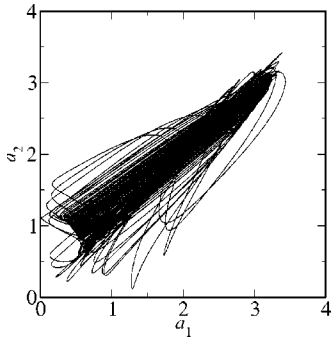

FIG. 10. Nearly amplitude-synchronous state for $\varphi=0.01\pi$, $\delta=0.6$.

of such solutions is $\varphi=0$. In this case, substituting $N:=N_1=N_2$ and $a:=a_1=a_2$ into Eq. (8) we obtain

$$a' = Na + \eta a \cos\Delta\psi, \tag{9}$$

$$N' = \varepsilon[J - N - (N+\nu)a^2], \tag{10}$$

$$\Delta\psi' = \delta - 2\eta \sin\Delta\psi. \tag{11}$$

The phase difference $\Delta\psi(t)$ can be explicitly found from Eq. (11). Namely, we have

$$\Delta\psi = 2\arctan\left[\frac{2\eta}{\delta} - \tanh\left(\frac{t}{2}\sqrt{4\eta^2-\delta^2}\right)\sqrt{\left(\frac{2\eta}{\delta}\right)^2-1}\right] \tag{12}$$

for $\delta<2\eta$ and

$$\Delta\psi = 2\arctan\left[\frac{2\eta}{\delta} + \tan\left(\frac{t}{2}\sqrt{\delta^2-4\eta^2}\right)\sqrt{1-\left(\frac{2\eta}{\delta}\right)^2}\right] \tag{13}$$

for $\delta>2\eta$. Solution (13) corresponds to a relatively small detuning. In this case, $\Delta\psi$ converges to the constant value $\Delta\psi\to\Delta\psi_0=2\arctan[2\eta/\delta-\sqrt{(2\eta/\delta)^2-1}]$ with $t\to\infty$ and system settles on a stable cw solution (cf. also Fig. 6 with $\varphi=0$). When the detuning δ becomes larger 2η, then $\Delta\psi$ behaves periodically (13) with the frequency $\omega_{syn}=\sqrt{\delta^2-4\eta^2}$. In this case, Eqs. (9) and (10) may be regarded as periodically forced system, which has a stable fixed point in the absence of forcing at $\eta=0$. Thus, we generally expect [24] that self-pulsations occur in Eqs. (9)–(11) with the same frequency ω_{syn}. Note that their period tends to infinity as $\delta\to 2\eta$.

To summarize, there exists for $\varphi=0$ a set of amplitude-synchronous periodic solutions for $\delta>2\eta$. We believe that approximate chaotic synchronization of intensities occurs as a result of further bifurcations of these solutions when φ is close to 0. As we will see in Sec. VI H there is a complicated dynamical mechanisms leading to the destabilization of self-pulsations. An example of such chaotic motion is shown in Fig. 10.

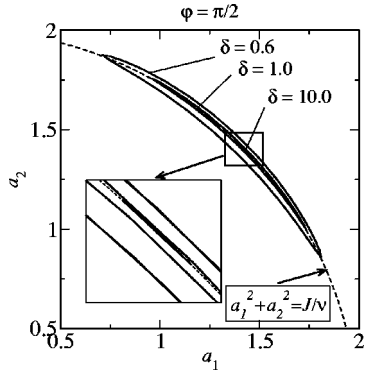

FIG. 11. "Inverse synchronization" for $\varphi=\pi/2$. The solutions are located near the arc $a_1^2+a_2^2=J/\nu$. Other parameters are $\eta=0.3$, $J=1$, $\varepsilon=0.03$, $\alpha=2$.

G. Inverse amplitude synchronization

When the propagation phase φ is close to $\pi/2$, we numerically observe solutions for which a_1 and a_1 behaves antiphase, cf. Fig. 9(c). Such a phenomenon was reported also in Ref. [14] and called inverse synchronization. To start with, let us substitute $\varphi=\pi/2$ into Eq. (8). We obtain the following system:

$$a_1' = N_1 a_1 - \eta a_2 \sin \Delta\psi,$$

$$N_1' = \varepsilon[J - N_1 - (N_1 + \nu)a_1^2],$$

$$a_2' = N_2 a_2 + \eta a_1 \sin \Delta\psi, \tag{14}$$

$$N_2' = \varepsilon[J - N_2 - (N_2 + \nu)a_2^2],$$

$$\Delta\psi' = \delta + (N_1 - N_2)\alpha + \eta\left(\frac{a_1}{a_2} - \frac{a_2}{a_1}\right)\cos \Delta\psi,$$

which again can be considered as a perturbed uncoupled system with coupling parameter η acting as a perturbation parameter. The unperturbed system (i.e., $\eta=0$) has an asymptotically stable fixed point $\hat{N}_1=\hat{N}_2=0$, $\hat{a}_1=\hat{a}_2=\sqrt{J/\nu}$. The perturbation term $\eta(a_2 \sin \Delta\psi, 0, a_1 \sin \Delta\psi, 0)^T$ is tangent to the arc $N_1=C$, $N_2=C$, $a_1^2+a_2^2=R^2$ with some fixed R and C. We numerically observe that the resulting oscillations are close to the arc with $R=\sqrt{J/\nu}$, and $C=0$, i.e., they appear around the point $\hat{a}_i, \hat{N}_i$, cf. Fig. 11. Note that the set $N_1=N_2=0$, $a_1^2+a_2^2=J/\nu$ is not invariant for Eq. (14) with nonzero ε.

Thus, we have observed that for two distinct cases $\varphi=0$ and $\varphi=\pi/2$ the coupling terms naturally appear in the dynamical equations (9)–(11) and (14) in such a way that for $\varphi=0$ they act along the diagonal $a_1=a_2$ and result in the appearance of amplitude-synchronous solutions. For $\varphi=\pi/2$ the coupling term in Eq. (14) acts transversely to the diagonal and tangentially to the arc $a_1^2+a_2^2=R^2$ and results in the appearance of the antiphase solutions.

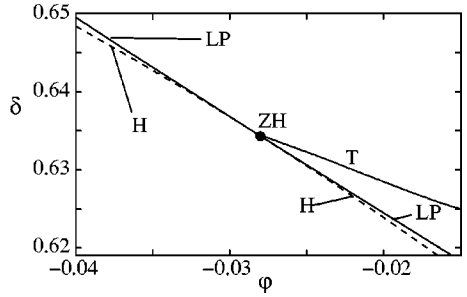

FIG. 12. Neighborhood of the zero-Hopf bifurcation. T denotes the Neimark-Sacker bifurcation curve emerging from the zero-Hopf point.

H. Appearance of chaotic oscillations near zero-Hopf bifurcation point

In the vicinity of the zero-Hopf bifurcation point, cf. Fig. 12, there is a branch of Neimark-Sacker bifurcations emerging from ZH point (see general case in Ref. [25]). When crossing this curve from above, the stable limit cycle undergoes Neimark-Sacker bifurcation. It is a general observation (cf. Ref. [25], p. 302) that the torus created by the Neimark-Sacker bifurcation exists only for parameter values near the corresponding bifurcation curve. If one moves away from the curve, the torus losses its smoothness and will be destroyed. The complete sequence of events is likely to involve an infinite number of bifurcations, since any weak resonance point on the Neimark-Sacker curve is the root of an Arnold phase-locking tongue. In view of this fact, we did not try to resolve the bifurcations numerically below the curve T in Fig. 12. Instead, for randomly chosen initial conditions, we calculated Lyapunov exponents for different parameter values. Figure 13 shows the parameter values for which the largest Lyapunov exponent is positive, i.e., the complex dynamics is present. We can see that, in particular, such region comes arbitrary close (with the given precision) to ZH point.

VII. THE CASE OF A SMALL DELAY

In this section we discuss some properties of the symmetric system with small delay,

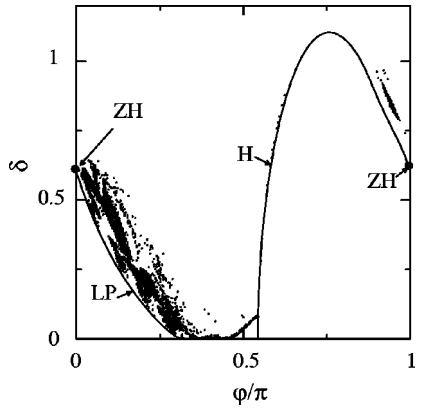

FIG. 13. Parameter values for which an attractor with positive largest Lyapunov exponent exists.

$$E_j'(t) = (1 + i\alpha)N_j(t)E_j(t) + \eta e^{-i\varphi}E_{3-j}(t-\tau),$$
$$N_j'(t) = \varepsilon[J - N_j(t) - \{N_j(t) + \nu\}|E_j(t)|^2], \quad j = 1,2, \tag{15}$$

and compare them with the corresponding properties of the instantaneously coupled system (4). The zero-delay approximation (4) would give a correct representation for the dynamics of delayed system (15), provided that the delay "is small enough." Mathematically, it can be regarded as existence of the stable finite-dimensional invariant manifold in the phase space of Eq. (15) for small enough τ such that the dynamics on this manifold is described by the system of ordinary differential equations (4) (cf. Ref. [26]). This implies that self-pulsations as well as more complicated dynamical regimes (bounded chaotic attractors) that have been discovered in Eq. (4) have their counterparts in Eq. (15). The main problem-specific question is then for which values of τ system (4) approximates reasonably (15). In this section, we give some partial answer to this problem concerning cw solutions.

The dynamics of Eq. (15) within the synchronization subspace $E_1 = E_2 := E$, $N_1 = N_2 := N$ is governed by the Lang-Kobayashi equation [17]

$$E' = (1 + i\alpha)NE + \eta e^{-i\varphi}E(t-\tau),$$
$$N' = \varepsilon[J - N - (N + \nu)|E|^2]. \tag{16}$$

The parameters of the synchronous cw solutions $E(t) = ae^{i\omega t}, N(t) = N = \text{const}$ of Eq. (16) satisfy the following set of equations (cf. Refs. [27,28]):

$$N = -\eta\cos(\varphi + \omega\tau),$$
$$\omega - \alpha N = -\eta\sin(\varphi + \omega\tau), \tag{17}$$
$$a^2 = (J - N)/(N + \nu).$$

One can obtain sufficient conditions for system (16) to have only one external cavity mode, i.e., a unique solution of Eq. (17). For this, we shall write the equation for ω as

$$\omega = -\eta[\alpha\cos(\varphi + \omega\tau) + \sin(\varphi + \omega\tau)]. \tag{18}$$

The saddle-node bifurcation, which gives rise to additional external cavity modes, can be identified (cf. Ref. [27]) as a double root of Eq. (18). Hence, differentiating it with respect to ω, we obtain

$$1 = \tau\eta[\alpha\sin(\varphi + \omega\tau) - \cos(\varphi + \omega\tau)].$$

It is clear that the condition

$$\tau\eta < \frac{1}{\sqrt{1 + \alpha^2}} \tag{19}$$

guarantees that a double root does not exist. Hence, the inequality (19) roughly provides the limit within which one might expect that the delay τ does not qualitatively change the dynamics within the synchronization (antisynchronization) subspace.

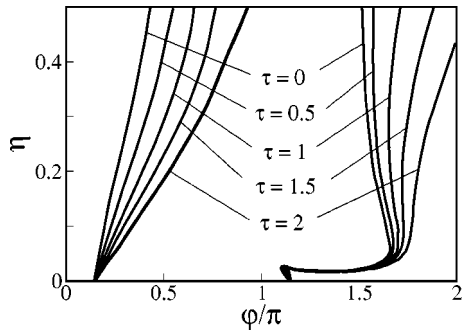

FIG. 14. Boundaries of the region for transverse stability of synchronous cw solutions of system (15) for different values of delay (similarly as in Fig. 1 without delay). The corresponding boundaries for antisynchronous cw solutions can be obtained by shifting along the φ axis by π.

The transverse stability of the unique synchronous cw solution is determined by the solutions of the characteristic equation

$$\chi_T^\tau(\Lambda) = [\Lambda^2 + 2\eta\cos\theta(e^{-\Lambda\tau} + 1)\Lambda + \eta^2(e^{-\Lambda\tau} + 1)^2] \times [\Lambda + \varepsilon(1 + S)] + 2\varepsilon S(\nu - \eta\cos\theta) \times [\Lambda + \eta(\cos\theta - \alpha\sin\theta)(e^{-\Lambda\tau} + 1)] = 0, \tag{20}$$

where

$$S := \frac{J + \eta\cos\theta}{\nu - \eta\cos\theta}$$

and

$$\theta := \omega\tau + \varphi.$$

The derivation is given in Appendix A. The condition $\chi_T^\tau(0) = 0$ determines the pitchfork and $\chi_T^\tau(i\Omega) = 0$ Hopf bifurcation, respectively. It turns out that for the values up to $\tau = 2$ the regions in the (φ, δ) parameter plane for the transverse stability of synchronous cw solution of Eq. (15) are qualitatively the same as in the case of zero delay (4). In Fig. 14 we plot the curves which delineate this stability region. All the remaining parameters are taken to be the same as in Fig. 1. The effect of delay for this range of τ can be only seen by continuous changing of the slope of the curves.

VIII. DISCUSSION AND CONCLUSION

In this paper we studied a model for a single-mode lasers which are optically coupled in a face to face configuration. The external cavity length is assumed to be short. We have derived conditions for the stability of synchronous cw solutions in terms of the coupling parameters. As a result of symmetry considerations, the properties of antisynchronous solutions can be determined by those of the synchronous. We have shown that when a detuning is present between two lasers, there exist stable stationary states under some parameter constellations, which can also be considered as a phase-locked states with $\Delta\psi = \text{const}$. Moreover, the connection between these states and the synchronous solutions of the

symmetric system (i.e., without detuning) is shown. We also investigate the mechanisms of appearance of self-pulsations, which are quasiperiodic solutions in terms of the original system (3) and represent periodic solutions of the reduced system (8). These mechanisms include Hopf bifurcation of the stationary phase-locked states and period-doubling bifurcation. We have shown that one of the organizing centers of chaotic pulsations in the considered system is a zero-Hopf (or Guckenheimer-Gavrilov) codimension-2 bifurcation point. From the point of view of modeling, we studied the possibility to use the model (3) with instantaneous coupling for the study of coupled semiconductor lasers with short external cavity.

In our analysis, we confined ourselves to the deterministic model. The spontaneous emission may cause additional effects to appear such as noise-induced chaos [29], coherence-resonance [30], or excitability [31]. We believe that there are certain topological configurations in the phase space that imply the existence of these effects. For example, one configuration assumes an S-shaped slow manifold like in Fitz-Hugh-Nagumo model, another [31] assumes that both separatrixes of a saddle point tend to an attractor, which is located nearby. In many cases, the necessary condition for the excitability is closeness to some bifurcation point or existence of a complicated topological structure in the phase space. Thus we may roughly anticipate that near the bifurcation lines and, especially, near the zero-Hopf bifurcation point, there is a rich potential for the necessary topological configurations to occur. We hope that the presented analysis will help one to localize such parameter regions.

ACKNOWLEDGMENTS

We wish to acknowledge useful discussions with M. Wolfrum, H.-J. Wünsche, A. Vladimirov, and N. Korneev. This work was supported by DFG (Sonderforschungsbereich 555 "Komplexe nichtlineare Prozesse").

APPENDIX A: DERIVATION OF THE CHARACTERISTIC EQUATIONS FOR SYNCHRONOUS SOLUTIONS

The algorithm for the derivation of the characteristic equations for the synchronous cw solutions of systems (15) and (4) is the same, therefore, we present here the derivation in detail for the delayed system (15). Finally, the characteristic equation for Eq. (4) will be obtained by setting $\tau=0$.

Let $E_1=E_2:=E_s e^{i\omega_s t}$, $N_1=N_2:=N_s$ be the synchronous cw solutions under consideration. By $F_{1,2}=(E_1\pm E_2)/2e^{-i\omega_s t}$ and $M_{1,2}=(N_1\pm N_2)/2$ we introduce new coordinates such that Eq. (15) takes the form

$$\dot{F}_{1,2}(t) = (1+i\alpha)[M_1 F_{1,2}(t) + M_2 F_{2,1}(t)] - i\omega_s F_{1,2}(t) \pm \eta e^{-i(\varphi+\omega_s\tau)} F_{1,2}(t-\tau),$$

$$\dot{M}_1 = \varepsilon[J - M_1 - (M_1+\nu)(|F_1|^2+|F_2|^2) - M_2(F_1\overline{F_2}+\overline{F_1}F_2)], \tag{A1}$$

$$\dot{M}_2 = \varepsilon[-M_2 - (M_1+\nu)(F_1\overline{F_2}+\overline{F_1}F_2) - M_2(|F_1|^2+|F_2|^2)].$$

F_1 and M_1 are the coordinates within the synchronization subspace, while the coordinates F_2 and M_2 are transversal to it [4,21], i.e., we have $F_2=0, M_2=0$ for synchronized solutions.

System (A1) is again autonomous due to the phase-shift invariance of the original system (15), and cw solution under consideration is transformed into the equilibrium $F_1=E_s$, $M_1=N_s$, $F_2=0$, $M_2=0$ with respect to it. We will linearize (A1) in the vicinity of such point [32]. To perform this, we first decompose

$$F_{1,2} = x_{1,2} + iy_{1,2}.$$

Denoting with

$$\vec{v} := (v_1, \ldots, v_6)$$

variations in $x_1, y_1, M_1, x_2, y_2, M_2$, respectively, we obtain a linearization of the form

$$\frac{d}{dt}\vec{v}(t) = A\vec{v}(t) + B\vec{v}(t-\tau),$$

with the 6×6 matrices A and B having the block structure,

$$A = \begin{pmatrix} A_1 & A_2 \\ A_2 & A_1 \end{pmatrix}, \quad B = \begin{pmatrix} B_1 & 0 \\ 0 & -B_1 \end{pmatrix}. \tag{A2}$$

At a synchronized state, we have $x_2=y_2=M_2=0$ and $M_1=N_{1,2}=:N$, and obtain

$$A_1 = \begin{pmatrix} N & \omega_s-\alpha N & x_1-\alpha y_1 \\ -(\omega_s-\alpha N) & N & \alpha x_1 + y_1 \\ -2\varepsilon x_1(N+\nu) & -2\varepsilon y_1(N+\nu) & -\varepsilon(1+x_1^2+y_1^2) \end{pmatrix}, \tag{A3}$$

$$B_1 = \begin{pmatrix} \eta\cos(\varphi+\omega_s\tau) & \eta\sin(\varphi+\omega_s\tau) & 0 \\ -\eta\sin(\varphi+\omega_s\tau) & \eta\cos(\varphi+\omega_s\tau) & 0 \\ 0 & 0 & 0 \end{pmatrix}. \tag{A4}$$

The coupling terms in A_2 disappear for synchronized cw states and the system splits into two invariant subspaces, corresponding to *synchronized* and transverse variations. As a consequence, the characteristic function can be factorized as $\chi^\tau(\Lambda)=\chi_L^\tau(\Lambda)\chi_T^\tau(\Lambda)$ with

$$\chi_L^\tau(\Lambda) = \det(\Lambda\, I - A_1 - e^{-\Lambda\tau}B_1) \tag{A5}$$

and

$$\chi_T^\tau(\Lambda) = \det(\Lambda\, I - A_1 + e^{-\Lambda\tau}B_1). \tag{A6}$$

Here I is identical 3×3 matrix. The function χ_L^τ is the characteristic function of the Lang-Kobayashi system (16) and has been investigated in Ref. [27]. It determines the stability properties of the synchronous cw solution of coupled system (2). The function χ_T^τ determines its transverse stability properties. Taking into account equations (17), we can rewrite transverse characteristic equations in terms of the parameters in the form (20).

Similarly, the characteristic equations for the transverse stability of synchronous solution to Eq. (4) have the form (6).

APPENDIX B: SET OF EQUATIONS FOR DETERMINING ASYNCHRONOUS cw SOLUTIONS

Here we obtain a set of equations for determining asynchronous cw solutions of Eq. (4). We also present an algorithm of reducing it to a single nonlinear equation with one unknown variable $\psi \in [0, 2\pi]$.

After substituting Eq. (7) into Eq. (3), we obtain the following set of equations with respect to unknowns $a_1, a_2, \psi, \omega, N_1, N_2$:

$$\begin{aligned} a_1 i\omega &= (1 + i\alpha)N_1 a_1 + \eta a_2 e^{-i(\psi+\varphi)}, \\ a_2 i\omega &= (1 + i\alpha)N_2 a_2 + \eta a_1 e^{i(\psi-\varphi)}, \\ J - N_1 &- (N_1 + \nu)a_1^2 = 0, \\ J - N_2 &- (N_2 + \nu)a_2^2 = 0. \end{aligned} \tag{B1}$$

In real form it reads

$$a_1 N_1 + a_2 \eta \cos(\varphi + \psi) = 0, \tag{B2}$$

$$a_1(\alpha N_1 - \omega) - a_2 \eta \sin(\varphi + \psi) = 0, \tag{B3}$$

$$a_2 N_2 + a_1 \eta \cos(\psi - \varphi) = 0, \tag{B4}$$

$$a_2(\alpha N_2 - \omega) + a_1 \eta \sin(\psi - \varphi) = 0, \tag{B5}$$

$$J - N_1 - (N_1 + \nu)a_1^2 = 0, \tag{B6}$$

$$J - N_2 - (N_2 + \nu)a_2^2 = 0. \tag{B7}$$

Since $a_1 \neq 0$, we may set $x = a_2/a_1$. In the following we perform a formal procedure without checking signs and zeros of some functions, in order to avoid additional nonessential details. As a result some spurious roots for new equation will appear which can be eliminated afterward. The system for unknowns $x, \psi, \omega, N_1, N_2$ has the form

$$N_1 + x\eta \cos(\varphi + \psi) = 0, \tag{B8}$$

$$(\alpha N_1 - \omega) - x\eta \sin(\varphi + \psi) = 0, \tag{B9}$$

$$xN_2 + \eta \cos(\psi - \varphi) = 0, \tag{B10}$$

$$x(\alpha N_2 - \omega) + \eta \sin(\psi - \varphi) = 0, \tag{B11}$$

$$\frac{(J - N_2)(N_1 + \nu)}{(J - N_1)(N_2 + \nu)} = x^2, \tag{B12}$$

where Eq. (B12) is obtained from Eqs. (B6) and (B7). Now we eliminate x from the following equations pairwise: (B8),(B9); (B10),(B11); (B8),(B10); and (B8),(B12). As a result we obtain equations for unknowns ψ, ω, N_1, N_2,

$$N_1 \sin(\varphi + \psi) + (\alpha N_1 - \omega)\cos(\varphi + \psi) = 0, \tag{B13}$$

$$N_2 \sin(\psi - \varphi) - (\alpha N_2 - \omega)\cos(\psi - \varphi) = 0, \tag{B14}$$

$$N_1 N_2 = \eta^2 \cos(\varphi + \psi)\cos(\psi - \varphi), \tag{B15}$$

$$\frac{(J - N_2)(N_1 + \nu)}{(J - N_1)(N_2 + \nu)} = \frac{N_1^2}{\eta^2 \cos^2(\psi + \varphi)}. \tag{B16}$$

N_1, N_2 can be determined using Eqs. (B13) and (B14):

$$N_1 = \omega/[\alpha + \tan(\varphi + \psi)], \tag{B17}$$

$$N_2 = \omega/[\alpha + \tan(\varphi - \psi)]. \tag{B18}$$

After substituting Eqs. (B17) and (B18) into Eq. (B15), ω can be expressed as a function of ψ:

$$\omega^2 = \eta^2 \cos(\varphi + \psi)\cos(\varphi - \psi) \times [\tan(\varphi + \psi) + \alpha][\tan(\varphi - \psi) + \alpha]. \tag{B19}$$

Final step is to substitute N_1 and N_2 from Eqs. (B17) and (B18) into Eq. (B16):

$$\frac{[J[\tan(\varphi + \psi) + \alpha] - \omega][\nu[\tan(\varphi - \psi) + \alpha] + \omega]}{[J[\tan(\varphi - \psi) + \alpha] - \omega][\nu[\tan(\varphi + \psi) + \alpha] + \omega]} = \frac{\eta^2}{\omega^2}\cos^2(\varphi + \psi)[\alpha + \tan(\varphi + \psi)]^2. \tag{B20}$$

After substituting Eq. (B19) into Eq. (B20), we arrive at a nonlinear transcendental equation for ψ. This equation can be treated numerically more easylly since ψ is determined within a bounded interval $(0, 2\pi)$.

[1] G. D. VanWiggeren and R. Roy, Int. J. Bifurcation Chaos Appl. Sci. Eng. **9**, 2129 (1999).

[2] I. Fischer, Y. Liu, and P. Davis, Phys. Rev. A **62**, 011801 (2000).

[3] M. Möhrle, B. Sartorius, S. Bauer, O. Brox, A. Sigmund, R. Steingrüber, M. Radziunas, and H. Wünsche, IEEE J. Sel. Top. Quantum Electron. **7**, 217 (2001).

[4] L. Pecora, T. Carroll, G. Johnson, D. Mar, and J. Heagy, Chaos **7**, 520 (1997).

[5] J. Javaloyes, P. Mandel, and D. Pieroux, Phys. Rev. E **67**, 036201 (2003).

[6] A. Hohl, A. Gavrielides, T. Erneux, and V. Kovanis, Phys. Rev. Lett. **78**, 4745 (1997).

[7] T. Heil, I. Fischer, W. Elsäßer, J. Mulet, and C. R. Mirasso,

Phys. Rev. Lett. **86**, 795 (2001).
[8] M. Peil, T. Heil, I. Fischer, and W. Elsäßer, Phys. Rev. Lett. **88**, 174101 (2002).
[9] I. V. Koryukin and P. Mandel, Phys. Rev. E **65**, 026201 (2002).
[10] C. Masoller, Phys. Rev. Lett. **86**, 2782 (2001).
[11] E. M. Shahverdiev, S. Sivaprakasam, and K. A. Shore, Phys. Rev. E **66**, 017206 (2002).
[12] J. K. White, M. Matus, and J. V. Moloney, Phys. Rev. E **65**, 036229 (2002).
[13] S. Sivaprakasam, E. M. Shahverdiev, P. S. Spencer, and K. A. Shore, Phys. Rev. Lett. **87**, 154101 (2001).
[14] S. Sivaprakasam, I. Pierce, P. Rees, P. S. Spencer, K. A. Shore, and A. Valle, Phys. Rev. A **64**, 013805 (2001).
[15] I. Wedekind and U. Parlitz, Phys. Rev. E **66**, 026218 (2002).
[16] T. Heil, I. Fischer, W. Elsäßer, B. Krauskopf, K. Green, and A. Gavrielides, Phys. Rev. E **67**, 066214 (2003).
[17] R. Lang and K. Kobayashi, IEEE J. Quantum Electron. **16**, 347 (1980).
[18] I. V. Koryukin and P. Mandel, IEEE J. Quantum Electron. **39**, 1521 (2003).
[19] J. Mørk, B. Tromborg, and J. Mark, IEEE J. Quantum Electron. **28**, 93 (1992).
[20] Y. C. Kouomou and P. Woafo, Phys. Rev. E **67**, 026214 (2003).
[21] S. Yanchuk, Y. Maistrenko, and E. Mosekilde, Chaos **13**, 388 (2003).
[22] S. Yanchuk, Y. Maistrenko, and E. Mosekilde, Physica D **154**, 26 (2001).
[23] E. Doedel, H. Keller, and J. Kernévez, Int. J. Bifurcation Chaos Appl. Sci. Eng. **1**, 493 (1991).
[24] C. Chicone, *Ordinary Differential Equations with Applications*, *Texts in Applied Mathematics* Vol. 34 (Springer, Berlin, 1999).
[25] Y. Kuznetsov, *Elements of Applied Bifurcation Theory*, *Applied Mathematical Sciences* Vol. 122 (Springer, Berlin, 1995).
[26] C. Chicone, J. Diff. Eqns. **190**, 364 (2003).
[27] M. Wolfrum and D. Turaev, Opt. Commun. **212**, 127 (2002).
[28] G. H. M. van Tartwijk and G. P. Agarwal, Prog. Quantum Electron. **22**, 43 (1998).
[29] S. K. Hwang, J. B. Gao, and J. M. Liu, Phys. Rev. E **61**, 5162 (2000).
[30] A. S. Pikovsky and J. Kurths, Phys. Rev. Lett. **78**, 775 (1997).
[31] B. Krauskopf, K. Schneider, J. Sieber, S. Wieczorek, and M. Wolfrum, Opt. Commun. **215**, 367 (2003).
[32] J. K. Hale and S. M. V. Lunel, *Introduction to Functional Differential Equations*, *Applied Mathematical Sciences* Vol. 99 (Springer, Berlin, 1993).